sustainability

MDPI

Article

Stochastic Optimal Operation of SOP-Assisted Active Distribution Networks with High Penetration of Renewable Energy Sources

Hongtao Li [1,†], Zijin Li [1,†], Bo Wang [1,†] and Kai Sun [2,3,*]

[1] State Grid Beijing Electric Power Research Institute, Beijing 100075, China; li.hongtao@163.com (H.L.); zijin1988@hotmail.com (Z.L.); sunyihannover@163.com (B.W.)
[2] State Key Laboratory of Power System Operation and Control, Tsinghua University, Beijing 100084, China
[3] Department of Electrical Engineering, Tsinghua University, Beijing 100084, China
* Correspondence: sun-kai@mail.tsinghua.edu.cn
† These authors contributed equally to this work.

Abstract: This paper introduces a mixed-integer convex model for optimizing the scheduling of soft open points (SOPs) integrated with energy storage (ES) in active distribution networks (ADNs) with high proportions of photovoltaic sources, designed to ensure zero risk of constraint violations. A stochastic optimization model for ADNs is proposed to maximize the benefits of SOPs while simultaneously minimizing system power losses, SOP power losses, voltage deviations, PV power curtailment, battery energy storage system (BESS) operation cost, and utility power purchase. Uncertainties in PV generation and load demand are considered by Monte Carlo simulation and k-means technologies. Finally, simulation cases from a 21-bus distribution network show that the curtailment of PV sources is minimized and the power fluctuations of the BESS are reduced in comparison to the case without SOP. Constraints in the nodal voltages, power outputs, energy balance, and power flow are all satisfied.

Keywords: active distribution networks; scenario generation and reduction; uncertainty; soft open point; economic power dispatch

Citation: Li, H.; Li, Z.; Wang, B.; Sun, K. Stochastic Optimal Operation of SOP-Assisted Active Distribution Networks with High Penetration of Renewable Energy Sources. *Sustainability* **2024**, *16*, 5808. https://doi.org/10.3390/su16135808

Academic Editor: Luis Hernández-Callejo

Received: 12 June 2024
Revised: 1 July 2024
Accepted: 2 July 2024
Published: 8 July 2024

1. Introduction

To decrease the use of fossil fuels and CO_2 emissions, the past decade has seen a rapid increase in the deployment of renewable distributed generation (DG). This growth, however, introduces difficulties for managing active distribution networks (ADN). On one hand, the mismatch between DG distribution and demand can cause reverse power flow and worsen voltage issues, potentially leading to the simultaneous need for DG curtailment and load shedding within a system. On the other hand, the unpredictable and variable nature of renewable energy means that errors in forecasting DG outputs are unavoidable, compounding the challenges of maintaining real-time power balance in ADNs [1].

Accommodating the growing demand and generation of power will necessitate significant investment in reinforcing networks and replacing aging assets, a process that is both expensive and time-intensive. As an alternative, leveraging the flexibility of DG, demand response, and network devices offers a strategy to manage network constraints in real-time, presenting a potentially more efficient and cost-effective approach [2,3].

Soft open points (SOPs) power electronic devices typically installed at the normally open junctions of electrical distribution networks and offer precise and flexible control over the power and voltage within these systems. With their superior real-time power management capabilities, SOPs have proven to be effective in addressing the various challenges associated with distribution networks [4]. These devices, integral to distribution-level power electronics, were developed and named the Siemens multifunctional power link (SIPLINK) by Siemens AG in Germany in 2001 [5]. However, the name SOP was first mentioned in reference [6], highlighting their role in replacing normally open points within distribution networks.

The core component of an SOP consists of two voltage source converters (VSCs) connected back-to-back [7,8]. By substituting the mechanical switch at a normally open point with an SOP, it becomes possible to maintain continuous power transfer between two busbars. Consequently, SOPs are valued for their ability to facilitate flexible interconnections, making them the optimal choice for addressing imbalances between generation and power demand, thereby enhancing the energy efficiency of ADNs [6,9].

The SOP device has been utilized to reduce losses and balance loads, with strategies developed for local voltage control to address distribution system fluctuations and optimization methods incorporating SOPs and energy storage to minimize losses and voltage deviations [10,11]. Robust optimization techniques have been proposed to manage PV output uncertainties and exploit SOPs' benefits fully, including strategies to lower operational losses, correct three-phase imbalances, and a dual-time-scale optimization approach for multi-terminal SOPs to simultaneously reduce system loss and voltage imbalance [12–14]. Reference [15] found that SOPs supported the economical operation of ADN, with network performance enhancements achieved by integrating SOP usage and network reconfiguration strategies. Moreover, reference [16] introduced a coordinated scheduling method for ADNs, leveraging SOP and Plug-in Electric Vehicles (PEVs) across multiple timescales. It optimizes operational efficiency and handles uncertainties through advanced programming techniques, demonstrated an effective performance on modified IEEE and real distribution systems and showcased significant operational improvements.

Research has underscored SOPs' pivotal role in enhancing ADN operations. The coordination of SOPs with Volt–Ampere Reactive (VAR) regulation methods has successfully mitigated voltage violations through a convex programming strategy detailed in [17]. These strategies predominantly depend on predictive data, neglecting the uncertainties of PV outputs. Given these uncertainties, relying solely on deterministic SOP operation strategies might exacerbate voltage instability issues. To refine SOP control strategies for optimal effectiveness, reference [18] integrated a chance-constrained optimization model to ideally allocate SOPs, DG, and capacitor banks. Reference [19] introduced a data-driven stochastic optimization to devise optimal SOP strategies for the least favorable probabilities. Moreover, a two-stage stochastic optimization model for a hybrid wind farm with hydrogen and energy storage systems is introduced in [20], demonstrating better performance when compared to Monte Carlo and deterministic approaches in handling uncertainties. For the optimal operation of integrated energy systems, a distributionally robust approach is proposed in [21] to address uncertainties arising from renewable energy resources, load demand, and energy prices. Despite the indeterminacy of scenario probabilities, the forecasted outcomes within these scenarios are fixed, making scenario selection crucial to the method's success. The necessity to analyze a broad array of scenarios also significantly increases the computational workload.

The strategies in the above-mentioned documents have had great contributions to the optimal operation of ADNs with the existence of SOPs. However, the majority of works have focused on a single objective such as power losses, power curtailments, social welfare, and voltage deviations. Therefore, this paper considers multiple optimization objectives including power transmission losses, voltage deviations, operation costs of distributed battery energy storage systems (BESSs) and SOPs, as well as utility power purchase objective.

The rest of the document is structured in the following way: Section 2 explains the models, distribution networks, BESS operation model, PV curtailment model, as well as loss model of SOPs with energy storage system. Section 3 lays out the main problem that this paper addresses, starting with a clear-cut, certain scenario before moving on to a sturdier, uncertainty-ready model. After that, Section 4 provides simulation case study to show how this all works in a real-world example, with discussion of the results of simulations based on this case study. The paper ends with the conclusions in Section 5.

2. System Optimization Model

This section introduces the model of an ADN with PV sources, BESS, and SOP with BESS. The operational model of the ADN includes the power flow model, the SOP model with power losses, BESS operational constraints in the SOP, the power loss model as part of the ADN operation model, and the active and reactive operation objectives and constraints for PV sources and BESS.

2.1. Linearized Power Flow Model

The power flow model of an ADN is linearized as a DistFlow model [22]:

$$\begin{cases} \sum_{k\in\mathcal{F}(i)} P_{ki}(t) = \sum_{j\in\mathcal{C}(i)} P_{ij}(t) - p_i(t) + r_{ki}\frac{P_{ij}^2(t)+Q_{ij}^2}{V_i^2(t)}, \\ \sum_{k\in\mathcal{F}(i)} Q_{ki}(t) = \sum_{j\in\mathcal{C}(i)} Q_{ij}(t) - q_i(t) + x_{ki}\frac{P_{ij}^2(t)+Q_{ij}^2}{V_i^2(t)}, \\ \forall i \in \mathcal{I}/\{0\}, \forall (i,j) \in \mathcal{B}, \forall t \in \mathcal{T}, \end{cases} \tag{1}$$

where $\mathcal{F}(i)$ is the index set that contains all father nodes of node i, and set $\mathcal{C}(i)$ is the set that contains all children nodes of node i. r_{ki} and x_{ki} are the resistance and reactance parameters of cable $(k,\ i)$, and $P_{k,i}$, $Q_{k,i}$ represent the active and reactive power of cable $(k,\ i)$, meanwhile $p_i(t)$, $q_i(t)$ are the active and reactive power injection/absorption at node i at time instant t. Additionally, expression $V_i(t)$ is the nodal voltage amplitude at node i. $\mathcal{I}$ is the set of all buses except the slack bus.

The nodal voltages at time instant t are presented as

$$\begin{aligned} V_j^2(t) = V_i^2(t) - 2\left(r_{ij}P_{ij}(t) + x_{ij}Q_{ij}(t)\right) \\ + \underbrace{\left(r_{ij}^2 + x_{ij}^2\right)\frac{\left(P_{ij}^2(t) + Q_{ij}^2(t)\right)}{V_i^2(t)}}_{l_{ij}(t)}, \forall (i,j) \in \mathcal{B}, \forall t \in \mathcal{T} \end{aligned} \tag{2}$$

where $V_j(t)$ is the nodal voltage amplitude of node j. It can be seen that nodal voltages are related to the active and reactive power flows $P_{k,i}(t)$, $Q_{ki}(t)$, inherent parameters r_{ki} and x_{ki}, as well as neighboring nodal voltage amplitudes $V_i(t)$, and transmission power loss $l_{ij}(t)$. Expression (1) and (2) represent the power flow model of a three-phase balanced power system. In this paper, only the three-phase balanced system is investigated.

2.2. Modeling of SOP

Soft open points (SOPs) in this paper are considered as the back-to-back voltage source converters (VSCs), as shown in Figure 1. As shown in Figure 1, SOPs are composed of two AC/DC converters, one capacitor, and a DC/DC converter, as well as a battery BESS [11]. In the distribution system, feeders are typically interconnected via normally open points (NOP) for basic operational connectivity. However, to enhance the flexibility in managing both active and reactive power flows, an advanced power electronic device known as the SOP has been introduced [6], replacing the traditional NOP setup, as illustrated in Figure 1. This advanced SOP device integrates two voltage source converters (VSCs) linked by a shared direct current (DC) connection. One VSC is designated for active–reactive power (PQ) control, regulating the SOP's active power transmission and the converter's reactive power output. The second VSC is tasked with voltage and reactive power (Vdc-Q) control, ensuring stable DC bus voltage while also contributing to reactive power management. The advanced VSC controller within the SOP device boasts the ability to independently adjust active and reactive power levels, showcasing a significant leap in power distribution control technology.

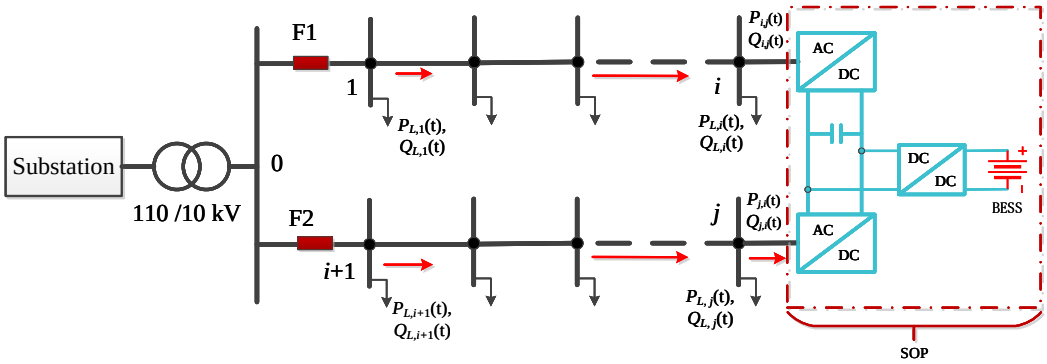

Figure 1. Active distribution network with SOP.

The power constraints of an SOP are formulated as

$$\begin{cases} P_i^{\mathrm{SOP}}(t) + P_j^{\mathrm{SOP}}(t) + P_i^{\mathrm{SOP,\,loss}}(t) \\ \qquad\qquad + P_j^{\mathrm{SOP,\,loss}}(t) = 0, \\ P_i^{\mathrm{SOP,\,loss}}(t) = A_i^{\mathrm{SOP}} \sqrt{\left(P_i^{\mathrm{SOP}}(t)\right)^2 + \left(Q_i^{\mathrm{SOP}}(t)\right)^2}, \\ P_j^{\mathrm{SOP,\,loss}}(t) = A_j^{\mathrm{SOP}} \sqrt{\left(P_j^{\mathrm{SOP}}(t)\right)^2 + \left(Q_j^{\mathrm{SOP}}(t)\right)^2}, \end{cases} \tag{3}$$

where $P_i^{\mathrm{SOP}}(t)$, $P_j^{\mathrm{SOP}}(t)$ are the active power of nodes i and j, and $P_i^{\mathrm{SOP,\,loss}}(t)$ and $P_j^{\mathrm{SOP,\,loss}}(t)$ are the power losses of AC/DC converters, respectively. A_i^{SOP} is the loss coefficient, and $Q_i^{\mathrm{SOP}}(t)$, $Q_j^{\mathrm{SOP}}(t)$ are the reactive power outputs of the SOP.

Additionally, the reactive power constraints and capacity constraints are formulated as

$$\begin{cases} P_i^{\mathrm{SOP,min}} \le P_i^{\mathrm{SOP}}(t) \le P_i^{\mathrm{SOP,max}}, \\ Q_j^{\mathrm{SOP,min}} \le Q_j^{\mathrm{SOP}}(t) \le Q_j^{\mathrm{SOP,max}}, \\ \sqrt{\left(P_i^{\mathrm{SOP}}(t)\right)^2 + \left(Q_i^{\mathrm{SOP}}(t)\right)^2} \le S_{ij}^{\mathrm{SOP}}, \\ \sqrt{\left(P_j^{\mathrm{SOP}}(t)\right)^2 + \left(Q_i^{\mathrm{SOP}}(t)\right)^2} \le S_{ij}^{\mathrm{SOP}}, \end{cases} \tag{4}$$

where $Q_i^{\mathrm{SOP,min}}$, $Q_i^{\mathrm{SOP,max}}$ are the minimal and maximal reactive power of the SOP, and S_{ij}^{SOP} is the capacity of the SOP connected between node i and node j.

The constraints of BESS integrated into the SOP are listed as

$$\mathrm{SOC}_i^{\mathrm{ESS,min}} \le \mathrm{SOC}_i^{\mathrm{ESS}}(t) \le SOC_i^{\mathrm{ESS,max}}, \tag{5}$$

$$\mathrm{SOC}_i^{\mathrm{ESS}}(t) = \mathrm{SOC}_i^{\mathrm{ESS}}(t-1) + P_i^{\mathrm{ESS}}(t) \times \Delta t, \tag{6}$$

$$P_i^{\mathrm{ESS}}(t) = \eta^{\mathrm{ch}} P_i^{\mathrm{ch}}(t) - P_i^{\mathrm{dch}}(t)/\eta^{\mathrm{dch}}, \tag{7}$$

where $\mathrm{SOC}_i^{\mathrm{ESS,min}}$, $\mathrm{SOC}_i^{\mathrm{ESS,max}}$ are the minimal and maximal values of state of charge (SOC) of the BESS in the SOP, $\mathrm{SOC}_i^{\mathrm{ESS}}(t)$ is the SOC of the BESS, and $P_i^{\mathrm{ESS}}(t)$ is the BESS power associated with the charging power $P_i^{\mathrm{ch}}(t)$ and discharging power $P_i^{\mathrm{dch}}(t)$ with an individual charging efficiency of η^{ch} and a discharging efficiency of η^{dch}. Δt is the power dispatching time unit.

For a given operation period, the SOC of the BESS should remain the same, which is formulated as

$$\mathrm{SOC}_i^{\mathrm{ESS}}(T_{end}) = \mathrm{SOC}_i^{\mathrm{ESS}}(T_{start}), \tag{8}$$

where T_{end} and T_{start} are the ending and starting time instants.

The optimization objective of SOPs is

$$F_{SOP}(t) = P_i^{\text{SOP, loss}}(t) + P_j^{\text{SOP, loss}}(t) + a_{sop}\left(P_i^{\text{ESS}}(t)\right)^2, \tag{9}$$

where a_{sop} is the economic parameter of the BESS in the SOP, which is the coefficient of the BESS operation cost.

2.3. Modeling of BESS

The operational constraints of a battery energy storage system (BESS) encompass several key factors: the mutual exclusion of charging and discharging states, limitations on energy capacity, and bounds on charging/discharging power outputs, as detailed in the following expressions:

$$\begin{cases} 0 \le P_i^{\text{ch}}(t) \le \alpha_i^{\text{ch}}(t) P_{\text{B},i}^{\max} \\ 0 \le P_i^{\text{dch}}(t) \le \alpha_i^{\text{dch}}(t) P_{\text{B},i}^{\max} \end{cases} \tag{10}$$

where $i = 1, \cdots, N_B$, $P_{\text{B}i}^{\max}$, $P_{\text{B}i}^{\min}$ are the maximal and minimal power outputs of ith BESS in ADN, N_B is the maximal number of distributed BESSs in ADN without the BESS integrated in the SOP. The binary variables $\alpha_i^{\text{ch}}(t)$ and $\alpha_i^{\text{dis}}(t)$ are used to control BESS charging and discharging behavior in a sequence. Therefore, it has

$$\alpha_{i,t}^{\text{ch}} + \alpha_{i,t}^{\text{dis}} \le 1 \tag{11}$$

The SOC constraints of distributed BESS are listed as

$$\begin{cases} \text{SOC}_i^{BESS}(t) = \text{SOC}_i^{BESS}(t-1) + \\ \qquad \left(\eta^{ch} P_i^{ch}(t) - \frac{1}{\eta^{dch}} P_i^{dch}(t)\right)\Delta t \\ \text{SOC}_i^{\text{BESS,min}} \le \text{SOC}_i^{\text{BESS}}(t) \le SOC_i^{\text{BESS,max}}, \\ SOC_i^{\text{BESS}}(T_{end}) = SOC_i^{\text{BESS}}(T_{start}). \end{cases} \tag{12}$$

Thus, the operation objective of BESS is formulated as

$$F_{BESS}(t) = \sum_{i=1}^{N_B} a_i \left(P_i^{\text{BESS}}(t)\right)^2, \tag{13}$$

where $P_i^{\text{BESS}}(t) = \alpha_i^{\text{ch}}(t) P_i^{\text{ch}}(t) + \alpha_i^{\text{dch}}(t) P_i^{\text{dch}}(t)$ is the BESS power, and $a_i > 0$ is the economic cost of ith BESS.

2.4. Modeling of PV Sources

The operation constraints of distributed PV sources in ADNs are formulated as

$$\begin{cases} P_{\text{PV}i}^{\min} \le P_i^{\text{pv}}(t) \le P_{\text{PV}i}^{\max}, \\ Q_{\text{PV}i}^{\min} \le Q_i^{\text{pv}}(t) \le Q_{\text{PV}i}^{\max}, \\ \sqrt{(P_i^{\text{pv}}(t))^2 + (Q_i^{\text{pv}}(t))^2} \le S_i^{\text{pv}}, \end{cases} \tag{14}$$

where $P_{\text{PV}i}^{\min}$, $P_{\text{PV}i}^{\max}$ are the minimal and maximal power outputs of PV sources. Usually, the minimal PV power outputs would be zero. PV sources work in maximal power point tracking (MPPT) control mode, therefore, the maximal PV power outputs depend on the solar radiation and surrounding environmental temperature. Aided by the PV power forecasting techniques, PV generation power could be curtailed. Thus, the operation model of PV sources is

$$F_{PV}(t) = \sum_{i=1}^{N_{PV}} a_{v,i} \left(P_i^{\text{pv}}(t) - P_i^{\text{pv,pref}}\right)^2, \tag{15}$$

where $P_i^{\text{pv,pref}}$ is the forecasted power of PV sources, $a_{v,i}$ is the economic cost, and N_{PV} is the number of PV sources.

2.5. Modeling of ADN

The operation constraints of ADN contain nodal voltage constraints and cable power flow constraints, which are presented as

$$\begin{cases} V_{\min} \le V_i(t) \le V_{\max}, \\ P_{i,j}^{\min} \le P_{ij}(t) \le P_{i,j}^{\max}, \quad \in \mathcal{B}, \forall t \in \mathcal{T}, \end{cases} \tag{16}$$

where $V_{\min}$, $V_{\max}$ are the minimal and maximal nodal voltages, and $P_{i,j}^{\min}$, $P_{i,j}^{\max}$ are the minimal and maximal power flow of branch $(i,\ j)$. To reduce the power transmission loss, the operation objective of ADN will be

$$\begin{aligned} F_{ADN}(t) = & \sum_{(i,j)\in|\mathcal{B}|} \left(r_{ij}^2 + x_{ij}^2\right) \frac{\left(P_{ij}^2(t) + Q_{ij}^2(t)\right)}{V_i^2(t)} \\ & + \sum_{t=1}^{T} \rho P_g(t), \end{aligned} \tag{17}$$

where $\forall (i,j) \in \mathcal{B}, \forall t \in \mathcal{T}$, and $|\mathcal{B}|$ is the cardinality of set $\mathcal{B}$.

In addition, the cost of purchasing power from the utility is designed as

$$F_{utility}(t) = \sum_{t=1}^{T} \rho P_g(t), \tag{18}$$

where ρ is the utility price and $P_g(t)$ is the power purchased from utility.

3. Optimization Model and Convexation

This section concludes the optimization objectives of the proposed models for ADN, which include SOP operation costs, PV operation costs (power curtailment costs), BESS operation costs, power losses of the ADN, and utility power purchase cost. To convexify the optimization model, a second-order cone program (SOCP) is adopted to relax the power losses.

3.1. Reformulation of Objectives

As discussed in Section 2.2, the optimization problem of ADN can be concluded as the minimization of power transmission losses, PV curtailments, BESS operation costs, and SOP operation costs, subjected to the various power inequality and equality constraints. Thus, the formulation of optimization problem of ADN with SOP will be

$$\min\ F = \sum_{t=1}^{T} \Big(F_{SOP}(t) + F_{PV}(t) + F_{BESS}(t) \tag{19}$$

$$+ F_{ADN}(t) + F_{utility}(t) \Big), \tag{20}$$

$$s.t. \begin{cases} (1),\ (2),\ (3),\ (4),\ (5),\ (6),\ (7), \\ (8),\ (10),\ (11),\ (12),\ (14),\ (16), \end{cases} \tag{21}$$

where T is the time instant. For one-day optimization, T will be $24 \times 4 = 96$, if the dispatching period is chosen as 15 min.

The use of the DistFlow model (1) introduces quadratic formulas through equality constraints, including the SOP's power constraints (3) and voltage constraints considering power loss (2). Consequently, this complexity turns the optimization problem into a non-convex one, complicating its resolution. Therefore, the proper approximation needs to be included. For the power flow model (1), the second-order cone program (SOCP)

model is adopted for the approximation. In the nonlinear term of power losses $l_{ij} = \left(r_{ij}^2 + x_{ij}^2\right)\frac{\left(P_{ij}^2(t)+Q_{ij}^2(t)\right)}{V_i^2(t)}$, reformulate $\frac{\left(P_{ij}^2(t)+Q_{ij}^2(t)\right)}{V_i^2(t)}$ as $I_{ij}^2(t)$; then, the relaxation will be

$$P_{ij}^2(t) + Q_{ij}^2(t) \le I_{ij}^2(t) \cdot V_i^2(t). \tag{22}$$

For SOP, the inequality constraint (3) should be relaxed. The proper approximation of power loss will be

$$\begin{cases} A_i^{\mathrm{SOP}}\sqrt{\left(P_i^{\mathrm{SOP}}(t)\right)^2 + \left(Q_i^{\mathrm{SOP}}(t)\right)^2} \le P_i^{\mathrm{SOP,\,loss}}(t), \\ A_j^{\mathrm{SOP}}\sqrt{\left(P_j^{\mathrm{SOP}}(t)\right)^2 + \left(Q_j^{\mathrm{SOP}}(t)\right)^2} \le P_j^{\mathrm{SOP,\,loss}}(t). \end{cases} \tag{23}$$

With these two relaxations, original equality constraints (2) and (3) will turn into inequalities, which will guarantee the feasibility of the optimization problem.

3.2. Scenario Generation and Reduction

Monte Carlo simulation (MCS) is used to deal with the uncertainties of PV generation and load demand. MCS is presented as a pivotal numerical method designed to capture the inherent randomness in various aspects of microgrid operation, such as load demand, renewable energy generation, and equipment reliability. MCS's primary role in this context is to simulate a wide range of possible future states, thus generating scenarios that reflect the uncertainty in these critical factors. The appeal of MCS lies in its straightforwardness and the directness of its application, marking it as distinctively less complex than alternative methodologies. This simplicity makes MCS an ideal choice for the second stage of microgrid planning. This stage is crucial for handling operational uncertainties following an initial phase that focuses on deterministic decisions related to infrastructure investments and installations.

A k-means clustering algorithm has been deployed to efficiently condense the generated scenarios, ensuring the preservation of their inherent characteristics without overwhelming decision-makers with data. This algorithm operates by grouping scenarios based on the similarity of their load demands and solar irradiance profiles. Each group, or cluster, is then represented by its centroid, calculated as the mean value of solar irradiance and load demands for the scenarios within that cluster. This process not only simplifies the dataset but also maintains the essential variability and characteristics of the original scenarios, facilitating a more manageable yet comprehensive analysis. A detailed calculated of scenarios and probability can be founded in reference [23].

With the generated scenarios, the optimization problem of ADN will be

$$\min\ F = \sum_{s=1}^{N_s}\sum_{t=1}^{T}\omega_s\Big(F_{SOP}(t) + F_{PV,s}(t) \tag{24}$$

$$+ F_{BESS}(t) + F_{ADN,s}(t) + F_{utility}(t)\Big), \tag{25}$$

$$s.t.\begin{cases} (1),\ (2),\ (3),\ (4),\ (5),\ (6),\ (7),\ (8), \\ (10),\ (11),\ (12),\ (14),\ (16),\ (22),\ (23) \end{cases} \tag{26}$$

where N_s is the total scenarios generated, and ω_s is the probability of s^{th} scenario. $F_{PV,s}(t)$ and $F_{ADN,s}(t)$ are the objective functions under the s^{th} scenario.

4. Numerical Results

To validate the proposed optimal operation strategy for ADN with an SOP, a 21-bus distribution system is adopted in a case study, as shown in Figure 2. The 10-kV distribution network contains six PV plants and a BESS installed at buses 3, 7, 9, 12, 16, and 20, respectively. Additionally, buses 20 and 14 are connected via an SOP, which is

integrated with a BESS to provide power support for the system. The system operates at a rated voltage of 11 kV, with a maximum branch flow capacity of 10 MVA. To ensure stability and efficiency within the network, the bus voltage levels are regulated to remain within a permissible range: the upper limit is set at 1.05 per unit (p.u.), and the lower limit is established at 0.95 p.u. This framework ensures that voltage levels at various buses within the network are maintained within a narrow window, promoting reliable and efficient power distribution.

PV sources and BESS units are integrated at designated nodes within the network, specifically at nodes [3, 7, 9, 13, 16, 20]. An SOP connection is established between nodes 14 and 20, with the relevant capacities detailed in Table 1. The maximum power outputs for the BESS units are set to $P_{\mathrm{B}}^{\max} = [1, 0.8, 1.2, 1.4, 1.0, 1.5]$ MW, and their minimum power outputs are defined inversely to their maximums, $P_{\mathrm{B}}^{\min} = -P_{\mathrm{B}}^{\max}$ MW. The BESS integrated within the SOP is configured to a maximum and minimum output of 1 MW and -1 MW, respectively.

The system's power factor is maintained at 0.95. Line characteristics, including resistance and reactance, are specified as $z = r + jx = 0.32 + j0.16\ (\Omega/\mathrm{km})$. The loss coefficient of SOP, denoted as A_i/A_j, is set at 0.02. As shown in Figure 3, total PV generation varies from zero to 5.5 MW, and the peak generation appears from 12 : 00 to 14 : 00. Load demand varies from 3.8 to 6.5 MW, and its peak demand occurs at 19 : 00 to 20 : 00.

Economic parameters for the PV sources and BESS, including those integrated with SOP, are outlined with cost coefficients $a = 1 \times 10^{-3}[0.11, 0.12, 0.09, 0.105, 0.13, 0.089, 0.11]$ S/kWh^2, and the utility price is set at 0.5 CNY/kWh. The simulation framework is implemented using MATLAB 2022b/CVX, and optimization problems are solved with Gurobi 10.0.0.

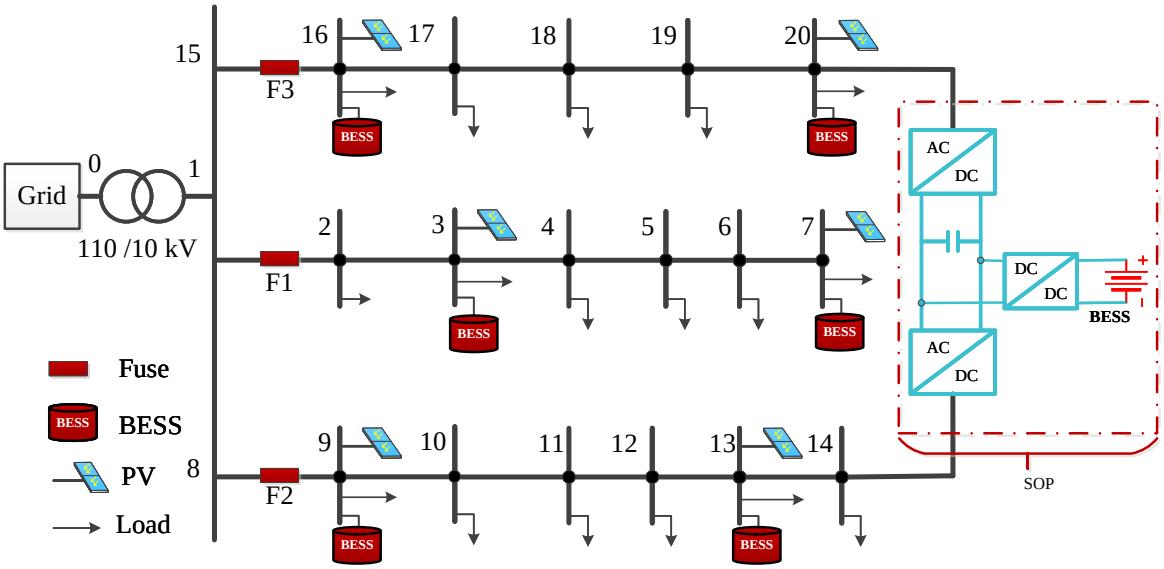

Figure 2. Simplified 21-bus distribution network with SOP, PV sources, and BESS.

Table 1. Capacities of distributed energy resources (DER) in ADN.

Source	PV (MW)	BESS (MWh)	SOP(MW)
1	0.9	5.0	1.0
2	1.1	4.0	/
3	0.7	6.0	/
4	0.8	7.0	/
5	1.2	5.0	/
6	0.9	7.5	/

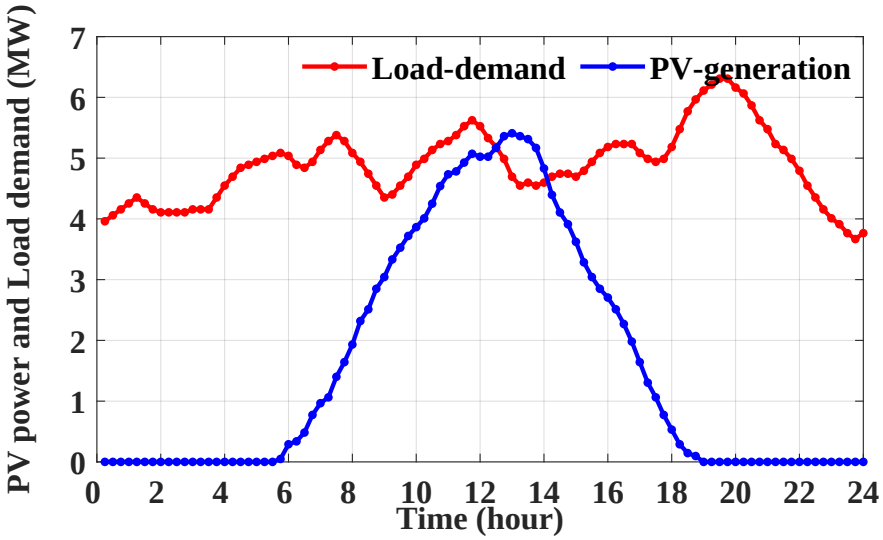

Figure 3. Total PV generation and load demand in ADN.

4.1. Simulation Results of ADN without SOP

This section examines the optimal operation of an ADN in the absence of an SOP. The dynamics of power and energy within the battery energy storage system (BESS) are depicted in Figure 4. Specifically, Figure 4a illustrates that the power output of the BESS varies between −0.8 MW and 0.7 MW. This is indicative of the charging phase, occurring from 8:00 to 17:00, during which the BESS absorbs energy, and the discharging phase, happening outside these hours, where the BESS releases energy. While charging, the BESS injects negative reactive power to regulate the nodal voltage within safe range. Conversely, during discharging, it supplies positive reactive power to the grid, ensuring the nodal voltage does not dip below acceptable levels. Additionally, Figure 4b demonstrates the state of charge (SoC) of the BESS over a 24 h cycle, confirming that the SoC remains consistently within the strategically designed range of 20% to 80%. Furthermore, the output power of each BESS vary from each other since the operation costs of BESS are different. Meanwhile, the reactive power outputs of the BESS are from −20 to 120 kVar to support system voltages, and the reactive power output of BESS at bus 3 is the highest during the peak hours (from 18:00 to 22:00). This is because the load demand of this branch is much higher than other branches and BESSs at this branch would generate more reactive power to support bus voltages.

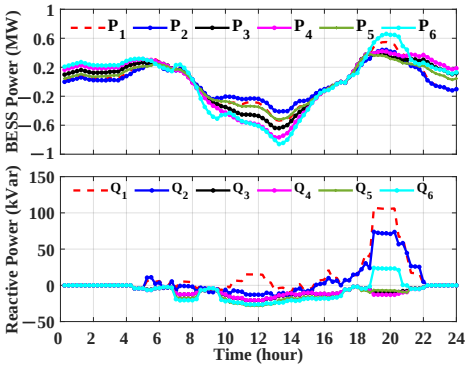

(**a**) Active and reactive power of BESS.

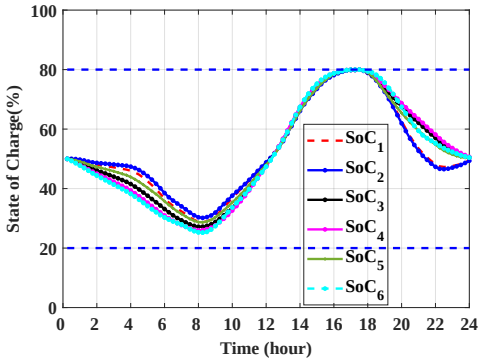

(**b**) State of charge of BESS.

Figure 4. Operation results of BESS.

Figure 5 presents the power outputs of photovoltaic (PV) sources, the power at the point of common coupling (PCC), and the nodal voltages of the network. As depicted in Figure 5a, from 6:00 a.m. to 7:00 p.m.—corresponding to daylight hours—PV sources

contribute active power to the grid, with values ranging from 0 to 1.1 MW, and each PV generate power according to its capacity from 0.6 MW to 1.2 MW. Notably, peak power outputs of PV sources occur between 12:00 p.m. and 2:00 p.m. During these daylight hours, PV sources also produce negative reactive power, thereby aiding in maintaining nodal voltages within the standard operational range. The reactive power generated by the PV sources fluctuates between −40 kVar and 0 kVar. However, the outputs of reactive power are different, which is caused by the power outputs constraints, power flow constraints, and load demand distribution in the system. Figure 5b illustrates that the active power at the PCC varies from 3.4 MW to 3.8 MW, while the reactive power remains approximately constant at 0.3 MVar, as indicated by the blue curve. Furthermore, Figure 5c confirms that nodal voltages at buses equipped with BESS are consistently within the acceptable range of 0.95 to 1.05 per unit (p.u.), ensuring stable operation within the network. Voltage constraints are satisfied because the PV, BESS and upper grid provide reactive power as well as PV active power curtailments. The curtailed power of PV sources are shown in Figure 5d, where it can be seen that the maximal curtailed power of PV reaches 85 kW during the peak time. The minimal curtailed power is still higher than 40 kW.

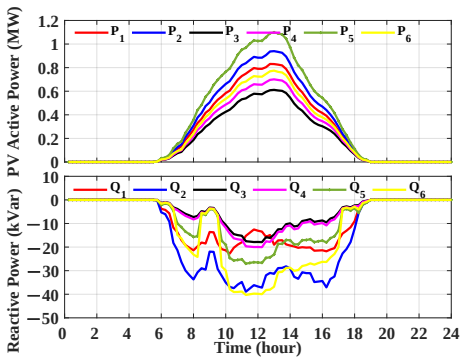

(**a**) PV power outputs.

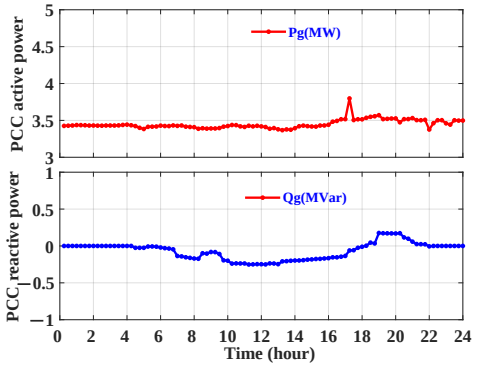

(**b**) Power outputs of PCC

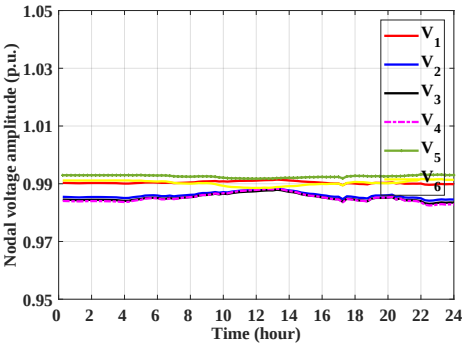

(**c**) Nodal voltages.

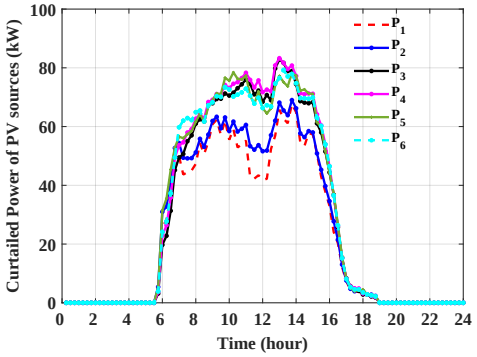

(**d**) Curtailed power of PV sources.

Figure 5. Operation results of ADN.

4.2. Simulation Results of ADN with SOP

This section examines the optimal operation of an active distribution network (ADN) with an SOP. The power outputs of a distributed BESS and SOP are shown in Figure 6. In Figure 6a, power outputs in the distributed BESS vary from −0.4 MW to 0.3 MW, and reactive power outputs are from 10 kVar to 110 kVar. With an SOP, the power outputs of BESS 1, 2, 3, 5 are close to each other; however, the power outputs of BESS 4 and BESS 6 installed at buses 14 and 20 are opposite during peak hours. This is because during the peak hours, load demand is transferred from bus 14 to bus 20. To conclude, the outputs of BESS are decided not only by operation costs but also by operation constraints of SOP.

Specially, the power outputs of the SOP and the BESS in an SOP are shown in Figure 6b, varying from −0.25 MW to 0.25 MW. Reactive power of the SOP stays close to −0.3 MVar, and reactive power of the BESS in an SOP is 0.5 MVar. Accordingly, the SoC of the distributed BESS varies in a small range, from 45% to 58%, since the variation in the distributed BESS is small, as shown in Figure 6c. The SoC of the SOP BESS is depicted in Figure 6d, demonstrating a fluctuation range from 45% to 55%. This variation is attributed to the smooth fluctuations in the power output of the BESS, which directly influences the SoC of the SOP.

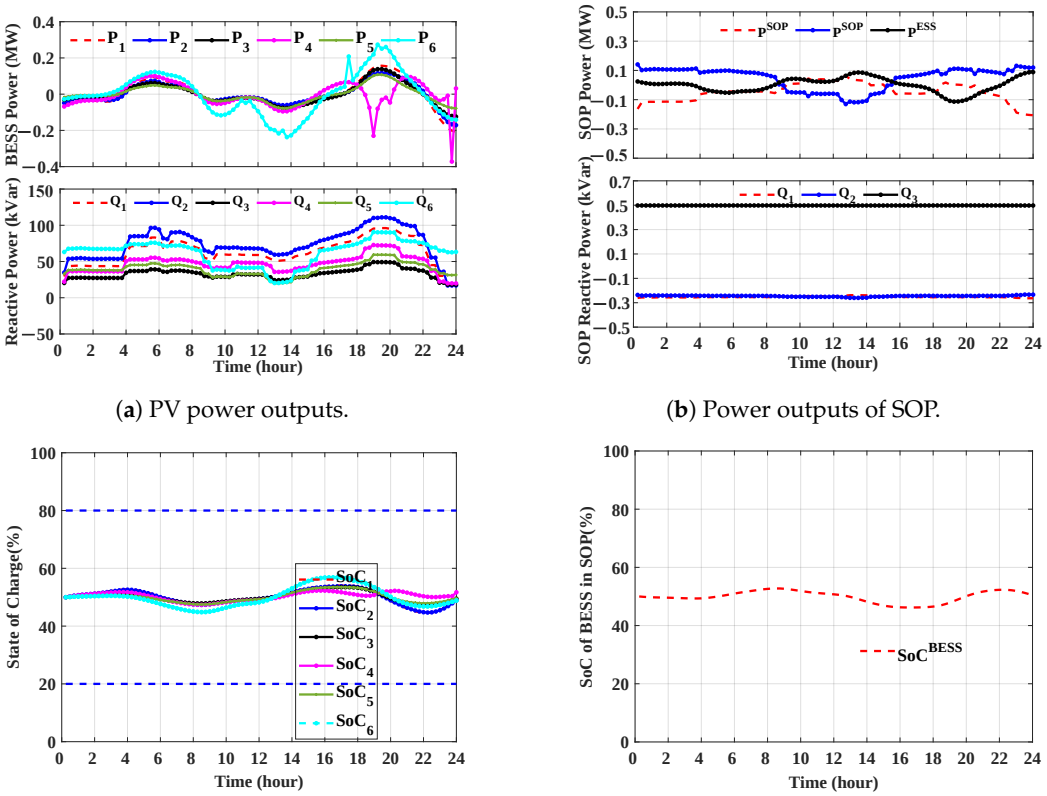

(**a**) PV power outputs.

(**b**) Power outputs of SOP.

(**c**) SoC of BESS.

(**d**) SoC of SOP-BESS.

Figure 6. Operation results of ADN with SOP.

Compared with BESS power outputs without an SOP, shown in Figures 4 and 6, the fluctuation BESS power output when an SOP is adopted is smaller than that without an SOP since the SOP transfers power between two different branches efficiently.

Additionally, PV power outputs are shown in Figure 7a, where their outputs vary from 0 to 1.2 MW; meanwhile, reactive power varies from zero to 30 kVar to support nodal voltages, and the curtailed power is decreased to about 5 kW, a large amount power decrease when compared with the power curtailment without an SOP, shown by Figure 6d. This means that PV power generation with an SOP is higher than PV generation without an SOP; in other words, the installation of an SOP increases the penetration of PV sources.

As seen in Figure 7c, utility power varies from 0 to 5.5 MW when an SOP is installed, and reactive power varies from 0.25 to 0 MVar. From 8:00 to 18:00, PV generation is shared by loads and BESS; therefore, it is indicated that load demand is locally balanced with the help of an SOP. Moreover, nodal voltages are still in the normal range of 0.98 to 1.01 p.u., as shown in Figure 7d.

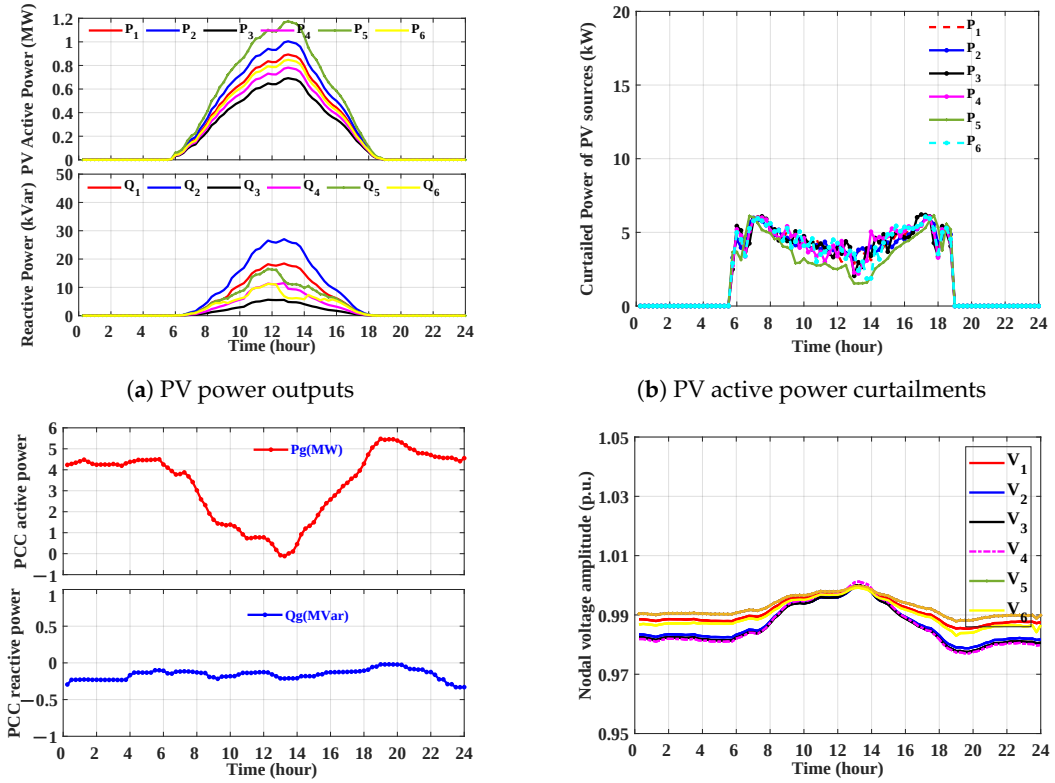

(**a**) PV power outputs

(**b**) PV active power curtailments

(**c**) The utility power

(**d**) Nodal voltages.

Figure 7. Operation results of ADN with SOP.

The SOP plays a pivotal role in enhancing the operational flexibility and efficiency of the distribution network, as validated by the results shown in Figures 4–7. It smooths BESS power outputs and reduces PV power curtailments. Compared to Figures 5d and 7b, the reduction in PV power curtailments is over 90% in general while still satisfying the operational constraints.

5. Conclusions

This paper introduces a sophisticated mixed-integer convex optimization framework specifically engineered for orchestrating the scheduling of SOPs seamlessly integrated with energy storage (ES) systems in ADNs that largely incorporate photovoltaic (PV) sources. The model is designed to eliminate any risk of constraint violations, ensuring a seamless operation. To further enhance the operational efficiency and sustainability of these networks, a comprehensive stochastic optimization strategy is proposed. This strategy is aimed at amplifying the utility and efficiency of SOPs while simultaneously aiming for a substantial reduction in system power losses, minimizing SOP-related power losses, curtailing voltage deviations, reducing the need for PV power curtailment, lowering the operational costs associated with BESS, and decreasing the necessity for utility power purchases.

To accommodate the inherent uncertainties associated with PV generation and load demand, the model employs advanced Monte Carlo simulation techniques coupled with k-means clustering technologies, providing a solution on robust optimization. Detailed simulation cases conducted on a structured 21-bus distribution network offer compelling evidence of the model's superior performance, with an over 90% percent reduction in PV power curtailment. The connection of SOPs into the network significantly minimizes the curtailments typically faced by PV sources and effectively dampens the power fluctuations experienced by BESS, showcasing a marked improvement over scenarios devoid of SOP integration. Moreover, the model ensures strict adherence to a set of critical operational constraints, including nodal voltage levels, precise power outputs, stringent energy balance

requirements, and fluid power flow dynamics, highlighting its comprehensive capability to enhance the resilience, efficiency, and reliability of ADNs with renewable energy sources.

Author Contributions: Conceptualization, H.L. and K.S.; methodology, K.S.; software, Z.L. and B.W.; validation, H.L., B.W. and Z.L.; formal analysis, K.S.; investigation, Z.L.; resources, B.W.; data curation, Z.L.; writing—original draft preparation, K.S.; writing—review and editing, K.S.; visualization, Z.L.; supervision, K.S.; project administration, H.L.; funding acquisition, H.L. All authors have read and agreed to the published version of the manuscript.

Funding: This work is supported by Science and Technology Project of SGCC (5400-202211507A-3-0-SF), China.

Institutional Review Board Statement: Not applicable.

Informed Consent Statement: Not applicable.

Data Availability Statement: The data supporting reported results are available from the corresponding author upon reasonable request.

Conflicts of Interest: Authors Hongtao Li, Zijin Li and Bo Wang was employed by State Grid Beijing Electric Power Research Institute. The remaining authors declare that the research was conducted in the absence of any commercial or financial relationships that could be construed as a potential conflict of interest.

References

1. Ahmed, R.; Sreeram, V.; Mishra, Y.; Arif, M. A review and evaluation of the state-of-the-art in PV solar power forecasting: Techniques and optimization. *Renew. Sustain. Energy Rev.* **2020**, *124*, 109792. [CrossRef]
2. Zhu, J.; Li, S.; Borghetti, A.; Lan, J.; Li, H.; Guo, T. Review of Demand-Side Energy Sharing and Collective Self-Consumption Schemes in Future Power Systems. *iEnergy* **2023**, *2*, 119–132. [CrossRef]
3. Oikonomou, K.; Parvania, M.; Khatami, R. Deliverable Energy Flexibility Scheduling for Active Distribution Networks. *IEEE Trans. Smart Grid* **2020**, *11*, 655–664. [CrossRef]
4. Fuad, K.S.; Hafezi, H.; Kauhaniemi, K.; Laaksonen, H. Soft Open Point in Distribution Networks. *IEEE Access* **2020**, *8*, 210550–210565. [CrossRef]
5. Jiang, X.; Zhou, Y.; Ming, W.; Yang, P.; Wu, J. An Overview of Soft Open Points in Electricity Distribution Networks. *IEEE Trans. Smart Grid* **2022**, *13*, 1899–1910. [CrossRef]
6. Bloemink, J.M.; Green, T.C. Increasing distributed generation penetration using soft normally-open points. In Proceedings of the IEEE PES General Meeting, Minneapolis, MN, USA, 25–29 July 2010; pp. 1–8. [CrossRef]
7. Cao, W.; Wu, J.; Jenkins, N.; Wang, C.; Green, T. Operating principle of Soft Open Points for electrical distribution network operation. *Appl. Energy* **2016**, *164*, 245–257. [CrossRef]
8. Ivic, D.; Stefanov, P. Control Strategy for DC Soft Open Points in Large-scale Distribution Networks with Distributed Generators. *CSEE J. Power Energy Syst.* **2022**, *8*, 732–742. [CrossRef]
9. Hou, Q.; Chen, G.; Dai, N.; Zhang, H. Distributionally robust chance-constrained optimization for soft open points operation in active distribution networks. *CSEE J. Power Energy Syst.* **2022**, 1–11. [CrossRef]
10. Li, P.; Ji, H.; Yu, H.; Zhao, J.; Wang, C.; Song, G.; Wu, J. Combined decentralized and local voltage control strategy of soft open points in active distribution networks. *Appl. Energy* **2019**, *241*, 613–624. [CrossRef]
11. Sarantakos, I.; Peker, M.; Zografou-Barredo, N.M.; Deakin, M.; Patsios, C.; Sayfutdinov, T.; Taylor, P.C.; Greenwood, D. A Robust Mixed-Integer Convex Model for Optimal Scheduling of Integrated Energy Storage-Soft Open Point Devices. *IEEE Trans. Smart Grid* **2022**, *13*, 4072–4087. [CrossRef]
12. Sun, F.; Ma, J.; Yu, M.; Wei, W. Optimized Two-Time Scale Robust Dispatching Method for the Multi-Terminal Soft Open Point in Unbalanced Active Distribution Networks. *IEEE Trans. Sustain. Energy* **2021**, *12*, 587–598. [CrossRef]
13. Ji, H.; Wang, C.; Li, P.; Ding, F.; Wu, J. Robust Operation of Soft Open Points in Active Distribution Networks With High Penetration of Photovoltaic Integration. *IEEE Trans. Sustain. Energy* **2019**, *10*, 280–289. [CrossRef]
14. Liu, G.; Sun, W.; Hong, H.; Shi, G. Coordinated Configuration of SOPs and DESSs in an Active Distribution Network Considering Social Welfare Maximization. *Sustainability* **2024**, *16*, 2247. [CrossRef]
15. Cao, W.; Wu, J.; Jenkins, N.; Wang, C.; Green, T. Benefits analysis of Soft Open Points for electrical distribution network operation. *Appl. Energy* **2016**, *165*, 36–47. [CrossRef]
16. Yang, X.; Xu, C.; Zhang, Y.; Yao, W.; Wen, J.; Cheng, S. Real-Time Coordinated Scheduling for ADNs With Soft Open Points and Charging Stations. *IEEE Trans. Power Syst.* **2021**, *36*, 5486–5499. [CrossRef]
17. Li, P.; Ji, H.; Wang, C.; Zhao, J.; Song, G.; Ding, F.; Wu, J. Coordinated Control Method of Voltage and Reactive Power for Active Distribution Networks Based on Soft Open Point. *IEEE Trans. Sustain. Energy* **2017**, *8*, 1430–1442. [CrossRef]

18. Zhang, L.; Shen, C.; Chen, Y.; Huang, S.; Tang, W. Coordinated allocation of distributed generation, capacitor banks and soft open points in active distribution networks considering dispatching results. *Appl. Energy* **2018**, *231*, 1122–1131. [CrossRef]
19. Wang, J.; Zhou, N.; Wang, Q. Data-driven stochastic service restoration in unbalanced active distribution networks with multi-terminal soft open points. *Int. J. Electr. Power Energy Syst.* **2020**, *121*, 106069. [CrossRef]
20. García-Miguel, P.L.C.; Zarilli, D.; Alonso-Martinez, J.; Plaza, M.G.; Gómez, S.A. Optimal Operation and Market Integration of a Hybrid Farm with Green Hydrogen and Energy Storage: A Stochastic Approach Considering Wind and Electricity Price Uncertainties. *Sustainability* **2024**, *16*, 2856. [CrossRef]
21. Yang, B.; Wang, Z.; Guan, X. *Optimal Operation of Integrated Energy Systems under Uncertainties: Distributionally Robust and Stochastic Methods*; Elsevier: Amsterdam, The Netherlands, 2023.
22. Baran, M.; Wu, F. Network reconfiguration in distribution systems for loss reduction and load balancing. *IEEE Trans. Power Deliv.* **1989**, *4*, 1401–1407. [CrossRef]
23. Pamshetti, V.B.; Singh, S.; Thakur, A.K.; Singh, S.P. Multistage Coordination Volt/VAR Control With CVR in Active Distribution Network in Presence of Inverter-Based DG Units and Soft Open Points. *IEEE Trans. Ind. Appl.* **2021**, *57*, 2035–2047. [CrossRef]